Materials Research Express

PAPER • OPEN ACCESS

Long single crystalline α-Mn_2O_3 nanorods: facile synthesis and photocatalytic application

To cite this article: Kalaiselvi Chandiran *et al* 2020 *Mater. Res. Express* **7** 074001

Materials Research Express

PAPER

Long single crystalline α-Mn_2O_3 nanorods: facile synthesis and photocatalytic application

Kalaiselvi Chandiran[1], **Ramesh Aravind Murugesan**[1], **Revathi Balaji**[1], **Nirmala Grace Andrews**[2], **Sudhagar Pitchaimuthu**[3] and **Krishna Chandar Nagamuthu Raja**[1]

[1] Department of Physics, School of Advanced Sciences, Vellore Institute of Technology, Vellore - 632 014, India
[2] Centre for Nanotechnology Research, Vellore Institute of Technology, Vellore - 632 014, India
[3] Multi-functional Nanocatalyst & Coatings Group, SPECIFIC, College of Engineering, Swansea University (Bay Campus), Swansea, SA1 8EN Wales, United Kingdom

E-mail: nkchandar@vit.ac.in

Keywords: hydrothermal method, α-Mn_2O_3 nanorods, photocatalytic, rhodamaine B, methylene blue

OPEN ACCESS

RECEIVED
19 March 2020

REVISED
22 June 2020

ACCEPTED FOR PUBLICATION
24 June 2020

PUBLISHED
3 July 2020

Abstract

Single crystalline cubic sesquioxide bixbyite α-Mn_2O_3 nanorods have been synthesized successfully by a simple, low cost, environmental benign hydrothermal route. As synthesized γ-MnOOH were calcined at 600 °C to obtain α-Mn_2O_3 nanorods, which were further subjected to various characterizations. The alpha manganese sesquioxide cubic bixbyite-type oxide formation was confirmed by the XRD studies. The surface morphology and elemental analysis were explored by SEM with EDX studies, respectively. High-resolution transmission electron microscopy HRTEM and SAED showed that the α-Mn_2O_3 nanorods were single crystalline and were grown along the *C*-axis of the crystal plane. The UV–visible spectrum indicated that the absorption was prominent in the ultraviolet region. In addition, PL spectrum result of α-Mn_2O_3 nanorods recommended possible photocatalytic applications. The photocatalyst ensures a new platform for the decolorization of dye molecules of the harmful cationic dyes like methylene blue and rhodamine B. Possible growth mechanism and photocatalytic dye degradation mechanism were proposed for synthesized α-Mn_2O_3 nanorods.

1. Introduction

Wastewater treatment and recycling are important concerns and researchers are looking forward to developing inexpensive and suitable technology for wastewater treatment. The wastewater has been treated by an advanced oxidation process, which is considered as attractive and effective technology in recent days [1–3]. Photocatalysis is a promising method, which can be used for the degradation of various organic and inorganic pollutants in wastewater [4, 5]. Nanosized semiconductor materials such as TiO_2, ZnO, CdS, ZnS, and WO_3 and Fe_2O_3 have the ability to play the role of higher photocatalytic activity. The two predominant photocatalytic materials found in the literature are considered as TiO_2 and ZnO because of their wide-bandgap semiconducting properties. But their photocatalytic activity is greatly decreased due to the rapid recombination rate of photoexcited electron-hole pairs [6, 7]. Recently, a few manganese oxide-based materials have been developed as alternative materials as a photocatalyst without any further modification. Manganese oxides have been the subject of much research due to the magnetic, electrical, and catalytic properties, structural variability, and different oxidation states and their broad range of physical and optical properties [8–10]. In nature, manganese oxide exhibits different oxidation states, which consists of MnO, MnO_2, Mn_2O_3, Mn_3O_4, and Mn_5O_8 [11]. In particular, the preparation of Mn_2O_3 has been attracted much research attention because of its environmentally friendly active catalyst for removing CO and NO from various sources.

There a variety of chemical and physical synthetic routes are available to synthesize Mn_2O_3 nanostructures, including hydrothermal, sol-gel, pulsed laser ablation, and co-precipitation methods [12–14]. The hydrothermal process offers several advantages over other methods such as lower energy consumption, reduced

environmental impact, controlled morphology, and high crystallinity [15]. At present, many works have been devoted to the synthesis and property studies of 1D Mn_2O_3 nanostructured materials, owing to their anisotropic dimension [16]. Many results in the literature support the existence of a large number of charge carriers on the active site of the nanostructures, which leads to a significant increase in the photocatalytic activity in comparison to nanoparticles in the spherical form [17]. Youcun Chena *et al* [18] Javed *et al* synthesized α-Mn_2O_3 nanorods [19] and nanowires employed by hydrothermal methods, Yong Cai *et al* synthesized α-Mn_2O_3 nanorods [12], Pijun Gong *et al* synthesized α-Mn_2O_3 nanorods [20] Yang Zhang *et al* synthesized α-Mn_2O_3 nanorods by hydrothermal treatment has been reported [21].

Gnanam *et al* synthesized (a-Mn_2O_3) nanodumb-bells had achieved the 71% degradation of the Remazol red B dye [22], Electrospun Mn_2O_3 nanowrinkles prepared by Mengzhu Liu *et al* showed catalytic effects on decomposition of methyl blue dye with H_2O_2 [1] and Jianhui Zhao *et al* employed a facile fabrication of novel Mn_2O_3 which degraded of ciprofloxacin at 94.7% [4]. Seldom research reports were published on the photocatalytic dye degradation for two cationic dye at different photocatalyst dosage for α-Mn_2O_3 nanorods. In addition, the formation and growth mechanism of α-Mn_2O_3 nanorods was also studied.

2. Experimental section

2.1. Materials

All chemical components used for the preparation of γ-MnOOH and α-Mn_2O_3 nanorods, used as without any further purification. Potassium permanganate [$KMnO_4$], and polyethylene glycol (PEG-400) were purchased from MERCK. Distilled water (DW) was used for the preparation of the aqueous solution. (PEG-400) non-ionic surfactant, low-cost, low toxicity, water-soluble organic polymer, and controls the size, and prevents agglomeration.

2.2. Synthesis of α-Mn_2O_3 nanorods

The α-Mn_2O_3 nanorods were prepared by hydrothermal method. 0.5 g of KMnO4 was dissolved in 70 ml of distilled water under magnetic stirring, and 1.9 ml of (PEG-400) was added to the above solution. The purple colour of the solution slowly changed to brown (indicating onset of the formation of manganese oxhydroxide). The manganese oxyhydroxide formed based on the redox reaction after that; the solution was transferred to a 100 ml capacity of Teflon-lined stainless steel autoclave, then hydrothermally treated at 150 °C for 15 h and then cooled to room temperature naturally. The resultant brown solid product was filtered, and vacuum dried at 90 °C for at 12 h. Finally, a brown powder (γ-MnOOH) was obtained that was calcined at 600 °C to form (α-Mn_2O_3) nanorods.

2.3. Characterization

The prepared (α-Mn_2O_3) nanorods were characterized by x-ray powder diffractometer ((XRD), which was obtained using Bruker, D8 Advance. FT-IR data of the product was collected using Fourier transform infrared (FT-IR) spectroscopy that was carried out on IR Affinity-1. The UV data was collected by UV–visible absorbance spectroscopy, and that was conducted using JASCO (V-670 PC). The room temperature of Photo-luminescence spectroscopy (RTPL), which was performed using F-7000 FL spectrophotometer. Morphology studies and chemical compositions were observed through scanning electron microscopy with energy-dispersive x-ray spectroscopy and elemental mapping (Zeiss EVO 18, Germany). High-resolution Transmission Electron Microscopy (HRTEM) was performed using FEI-TECNAIG2-20 TWIN at an operating voltage of 100kv and Bruker EDX with LN2 free detect. Photocatalytic dye degradation application was carried out by Mercury UV light source.

2.4. Photocatalytic measurements

The decolorization of dye molecules reaction was performed by Sankyo Denki Twelve numbers of 8W Mercury UV lamps of 254–365 nm wavelength. The change in the absorbance spectra of Methylene Blue (MB) and Rhodamine B (RB) with various irradiation times were determined using ultraviolet (UV) light source Typically, 6.5 mg of photocatalyst (α-Mn_2O_3) were added to the 100 ml of the aqueous solution of the MB, and 4.5 mg of photocatalyst added to the 100 ml of RB dye. Prior to the irradiation, the suspension was magnetically stirred in the dark for 30 min afterward; the suspensions were irradiated by a UV light source. At given irradiation time, the photo-reacted suspension (3 ml) was taken, and the suspension was analyzed by using a UV-vis spectrophotometer (MODEL: Specord 201 plus).

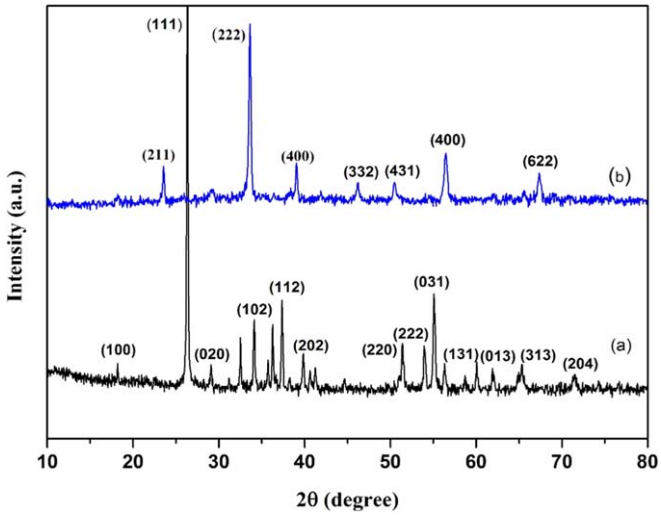

Figure 1. XRD patterns of the as-prepared (a) γ-MnOOH, and (b) α-Mn_2O_3 nanorods.

3. Result and discussion

3.1. Structural analysis

The XRD diffraction patterns of as-prepared γ-MnOOH and calcined α-Mn_2O_3 nanorods are in figure 1. All the diffraction peaks can be indexed to the monoclinic phase of γ-MnOOH figure 1(a). The strong and sharp diffraction patterns can be compared with a standard value of JCPDS file no 41-1379. Figure 1(b) the XRD pattern of the calcined (at 600 °C) sample confirms the bixbyite cubic phase of α-Mn_2O_3 nanorods. The peaks observed at $2\theta = 23.2°, 32.9°, 38.2°, 45.3°, 49.3°, 55.1°$ and $65.7°$, which can be attributed to the (211), (222), (400), (332), (431), (440) and (622) plans for α-Mn_2O_3 nanorods. (JCPDS 41-1442) [23–25]. There are no other diffraction peaks corresponding to impurities, indicating the high purity of the α-Mn_2O_3 nanorods. The average crystallite size D in nm was estimated using the Debye–Scherrer formula, which is $D = K\lambda/\beta \cos(\theta)$ where λ is the wavelength of the incident X-ray beam (1.5406 Å), β is the full width at half maximum (FWHM in radian) of the diffraction peak, θ is the Bragg diffraction angle, and k is Scherrer constant. The estimated average crystallite size of α-Mn_2O_3 nanorods was 31 nm. The lattice parameter of the cubic phase was calculated by using the combined formula of Bragg and the interplanar distance of the cubic structure $a = 0.9423$ nm.

$$\lambda = \frac{\sqrt{h^2 + k^2 + l^2}}{2 \sin \theta} \tag{1}$$

The x-ray density for a cubical system can be calculated using the $Dx = zM/NV$ formula, where z is the number of atoms per unit cell, M is the molecular weight, N is Avogadro's constant and V is the volume of the unit cell. The x-ray density calculated value was (Dx) is 5.0131 g cm^{-3} for α- Mn_2O_3 nanorods. Further, the specific surface area (SSA) of the α-Mn_2O_3 nanorods has been calculated with $S_a = 6/D\,Dx$ formula [23, 26]. The estimated value of SSA is 38.60×10^4 cm^2 g^{-1} for α-Mn_2O_3 nanorods.

3.2. Surface morphology analysis

Figures 2(a)–(c) shows the morphologies of the α-Mn_2O_3 nanorods at different magnifications. The samples clearly reveal the presence of a large quantity of α-Mn_2O_3 nanorods aligns in the random orientation. Figures 2(d), (e) shows the elemental mapping of α-Mn_2O_3 nanorods. Figure 2(f) shows the EDX pattern, which designates the purity of the α-Mn_2O_3 nanorods by indicative of only Mn and O. The stoichiometrical atomic percentage of Mn is 36% and O is 64%. From TEM images, it can be seen that the α-Mn_2O_3 sample displayed rod-like morphology. The single nanorods were randomly selected, which has a diameter of 318.4 nm and length in the range of 8.15 μm. The figure 3(e) is attributed to SAED consists of spots, which are identified as the diffraction from cubic single crystalline α-Mn_2O_3 nanorods. It is in good agreement with the results obtained from the XRD pattern [24]. The HRTEM images figure 7(d) show well-defined lattice fringes of α-Mn_2O_3 nanorods. It is indicating the single crystallinity of the nanorods. The interplanar spacing of fringes measured to be 0.368 nm, which corresponds to the (211) planes of α-Mn_2O_3 nanorods. It further confirmed the single-crystalline nature of the α-Mn_2O_3 nanorods, and growth along the *c*-axis. Figure 6(f) showed the uniform distribution like Mn and O throughout the α-Mn_2O_3 nanorods.

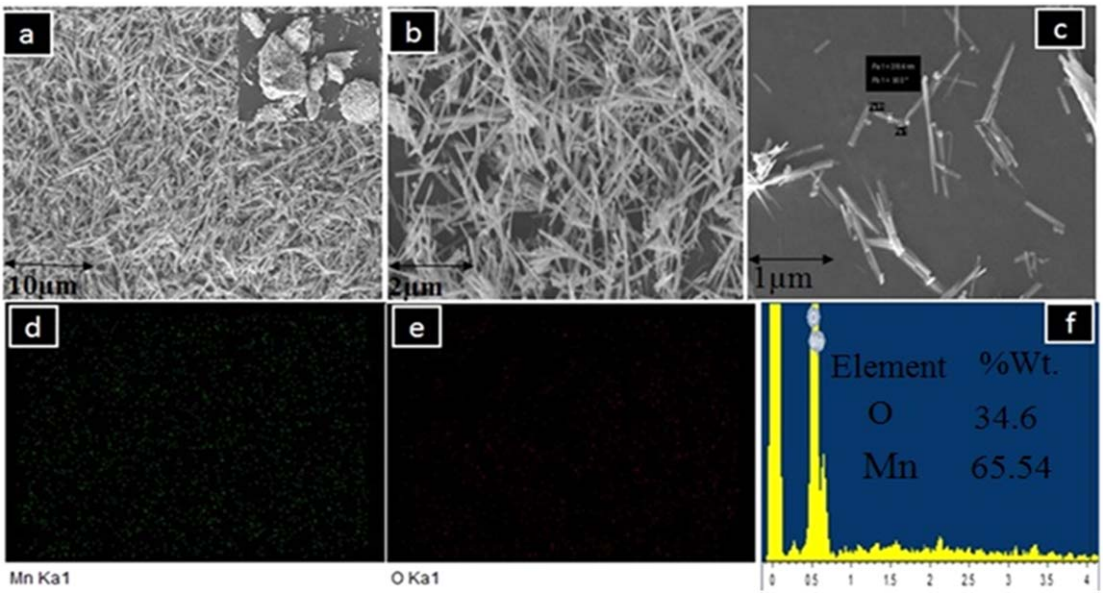

Figure 2. (a)–(c) SEM images of the α-Mn_2O_3 nanorods at different magnification. (d), (e) Elemental mapping of α-Mn_2O_3 nanorods. (f) EDX analysis of α-Mn_2O_3nanorods.

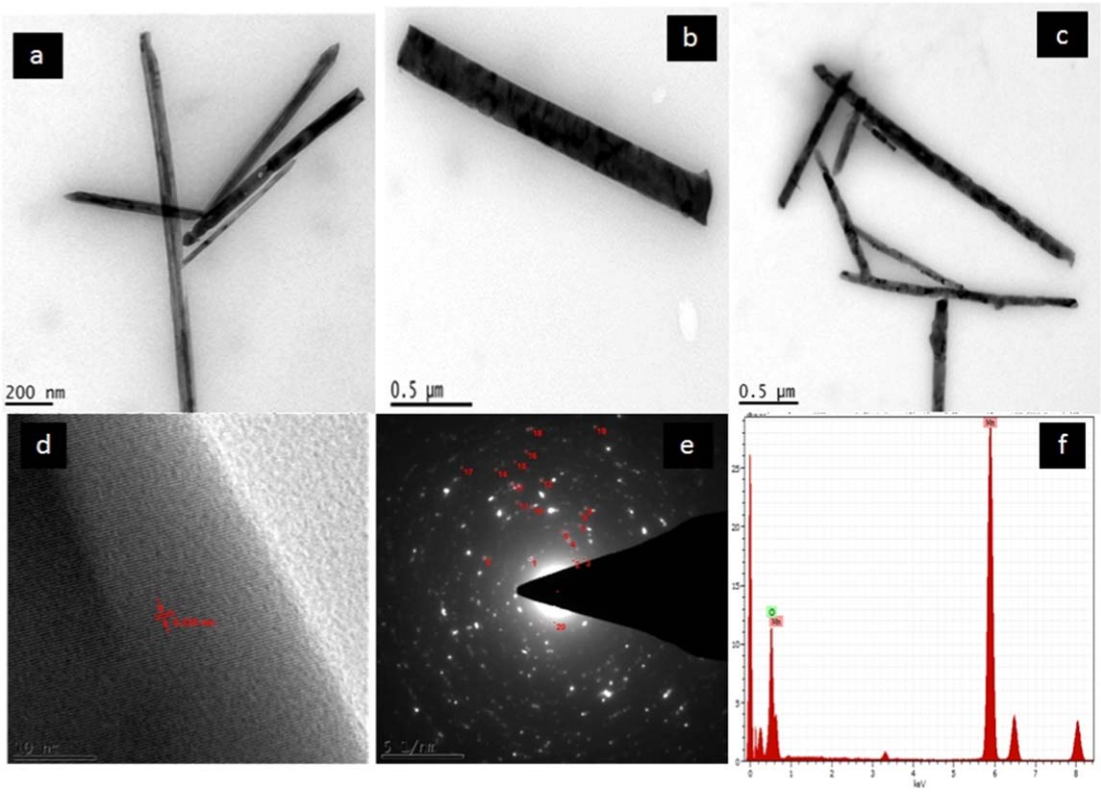

Figure 3. (a)–(c) TEM images of α-Mn_2O_3 nanorods at different magnification. (d) HRTEM image. (e) SEAD image and (f) EDX.

3.3. The growth mechanism of α-Mn_2O_3 nanorods

The growth mechanism of α-Mn_2O_3 nanorods illustrated in figure 4. The growth mechanism of α-Mn_2O_3 nanorods fully covered by nucleation, crystal growth, coalescence, oriented attachment. A large quantity of nanorods is formed by coalescing of nanoparticles together due to oriented attachment. Oriented attachment mechanism could be described as a self-organised arrangement of neighboring nanoparticles, so that they share an identical crystallographic configuration. When the crystallographic orientation is encountered, these nanoparticles were merging together [27]. This favorable process reduces the overall surface energy due to the

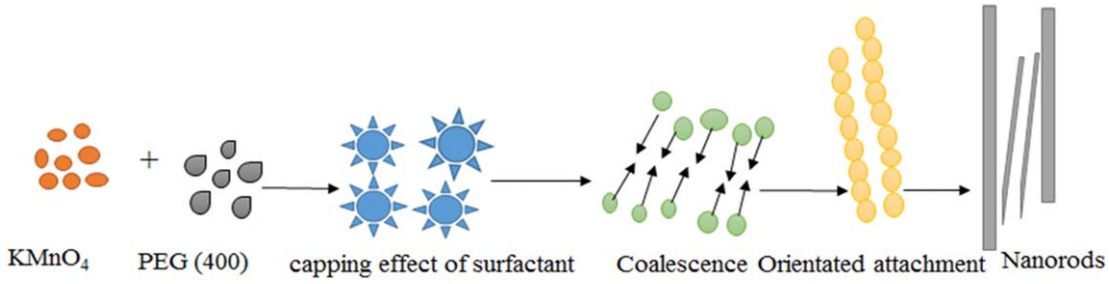

Figure 4. Schematic representation of the possible growth of α-Mn_2O_3 nanorods.

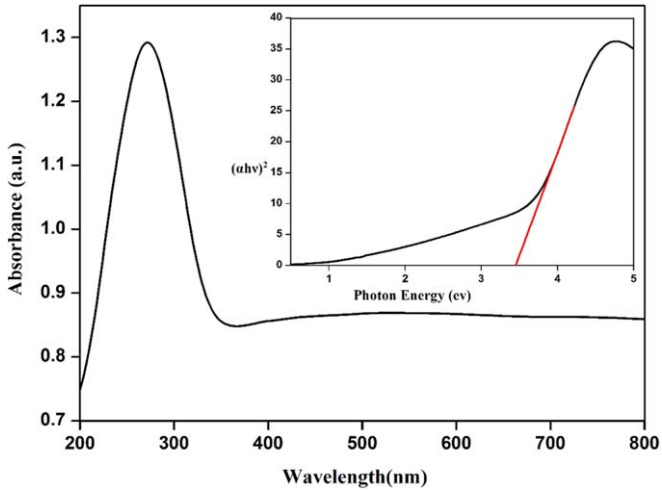

Figure 5. The UV-absorption spectrum of α-Mn_2O_3 nanorods.

elimination of energy associated with unsatisfied bonds [28]. A decrease in the length of the α-Mn_2O_3 nanorods could be explained by the limited lateral aggregation of nanoparticles. It may be possible to explain the sharp tip of some α-Mn_2O_3 nanorods arises because lower the surface energy and surface diffusion happened during the growth of the nanostructures [29].

3.4. Optical absorption analysis

UV–visible absorption spectrum of α-Mn_2O_3 nanorods were plotted in figure 5(a). A well-defined sharp and strong absorbance peak located at 300 nm due to the electron excitation from filled to the empty band was observed in $\pi \rightarrow \pi^*$ electronic transition [14]. The energy bandgap of the sample was calculated using the Tauc expressed in a relation between the absorption coefficient (α) and the energy of the photon ($h\nu$) as follows,

$$(\alpha h\nu)^2 = (h\nu - E_g)^n \quad (2)$$

It reveals that the obtained plotting gives to the linear portion of the curves in a certain region. The energy bandgap (Eg) was estimated using the intercept of the linear portion of the curve $(\alpha hv)^2$ versus ($h\nu$) shown in the inset of figure 6(b) and was found energy bandgap was 3.4 eV. This value is reported in the early reports of α-Mn_2O_3 nanorods [8]. The absorption edge and bandgap of α-Mn_2O_3 nanorods showed that photocatalytic reaction under UV conditions. Especially in the light wavelength range is 300 nm in photocatalytic application. Thus, it was necessary to understand its optical property and band structure.

3.5. Photoluminescence properties

The room temperature PL spectrum of the α-Mn_2O_3 nanorods was examined using the Xe excitation source with excited wavelength at 300 nm is shown in figure 6. It can be seen that the PL spectrum of α-Mn_2O_3 nanorods exhibits a broad blue emission band [21]. The broad blue band emission is due to the presence of oxygen vacancies that oxygen vacancies generally act as a deep defect the intrinsic point defect levels confined between the Mn 3d band, and O 2p band can result in a broader blue emission ban. In conclusion, our PL results

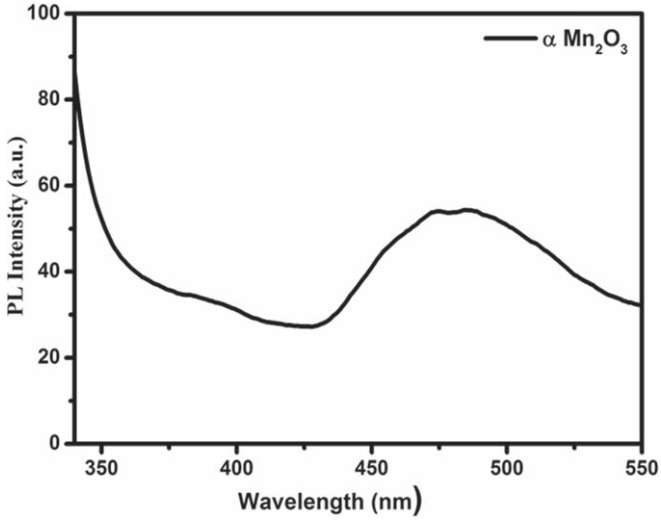

Figure 6. PL spectrum of the α-Mn_2O_3 nanorods.

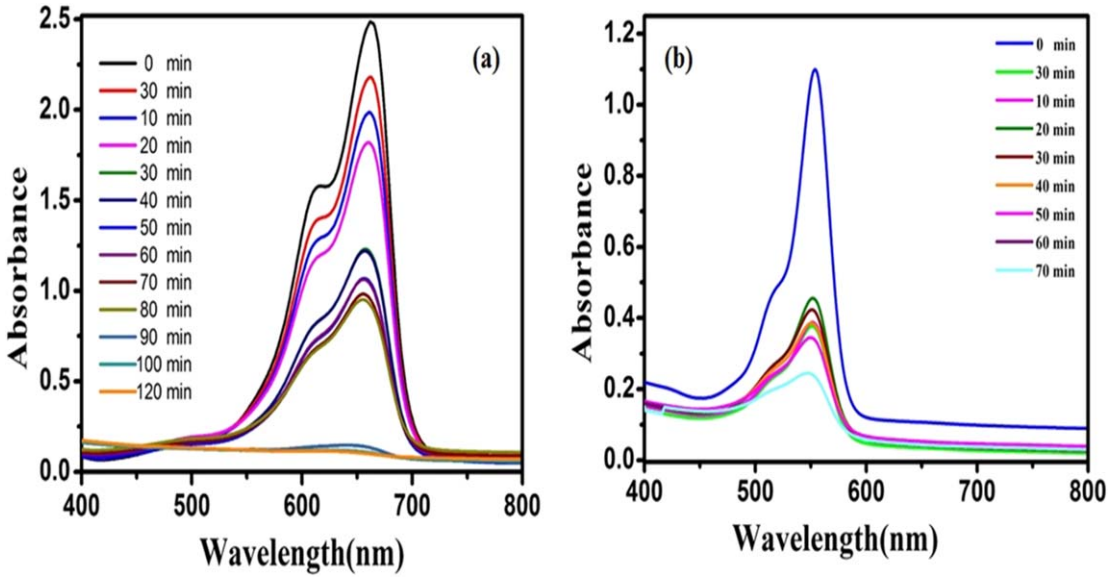

Figure 7. (a) UV-Visible absorption for the degradation of Methylene Blue. (b) Rhodamine B in the presence of α-Mn_2O_3 nanorods.

have evidenced the presence of vacancy in oxygen. In addition, many literature studies report oxygen vacancy was increased the photocatalytic reaction [30].

4. Photocatalytic dye degradation

The efficient photocatalytic activity of α-Mn_2O_3 nanorods was evaluated by the degradation of methylene blue (MB) and rhodamine B (RB) under UV illumination at different irradiation times. The decolorization of dye molecules efficiency was calculated using the formula $E\% = (1-C/Co)^{*}100$, where C is the residual concentration of MB and RB at different illumination time intervals. Co is the concentration of the MB and RB before illumination [31]. Figures 7(a) and (b) reports the presence of photocatalyst with (MB) and (RB) under UV lamp conditions, respectively. As the irradiation time increases, the maximum absorbance peak decreases slowly. This observation denotes that the concentration of the MB and RB decreases.

Figure 7(a) shows the complete dye degradation at 120 min for MB. Figure 7(b) rhodamine B (RB) absorbance peak was completely decreased at 70 min that indicates the total degradation of MB and RB dye and also designates the destroyed double bond of the chromophore [32]. In order to study the effect of α-Mn_2O_3 photocatalyst on RB and MB, the blank without photocatalyst was also tried, which were presented in

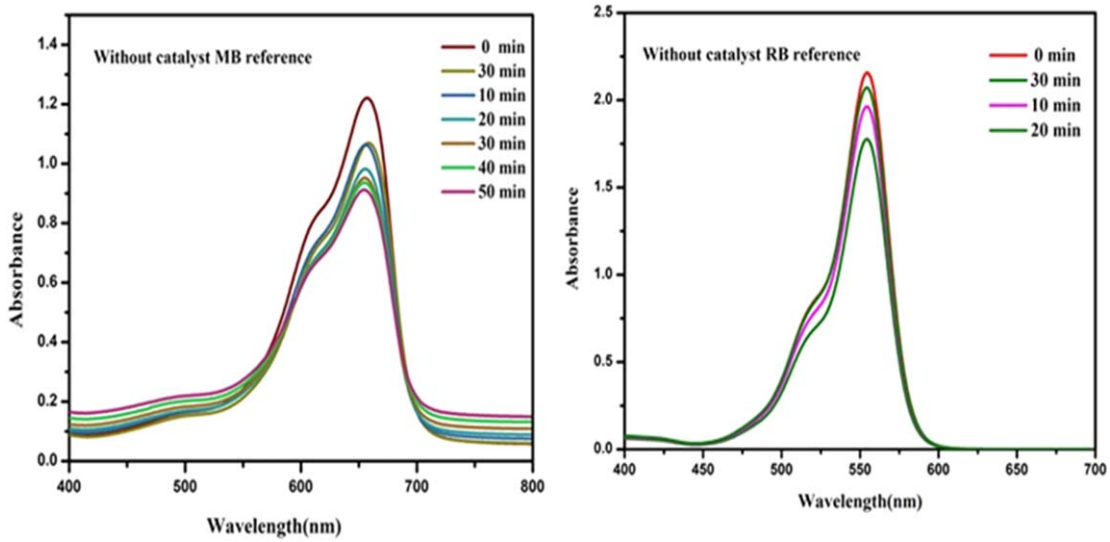

Figure 8. (a), (b) UV-Visible absorption spectra of blank Methylene Blue and Rhodamine B solution.

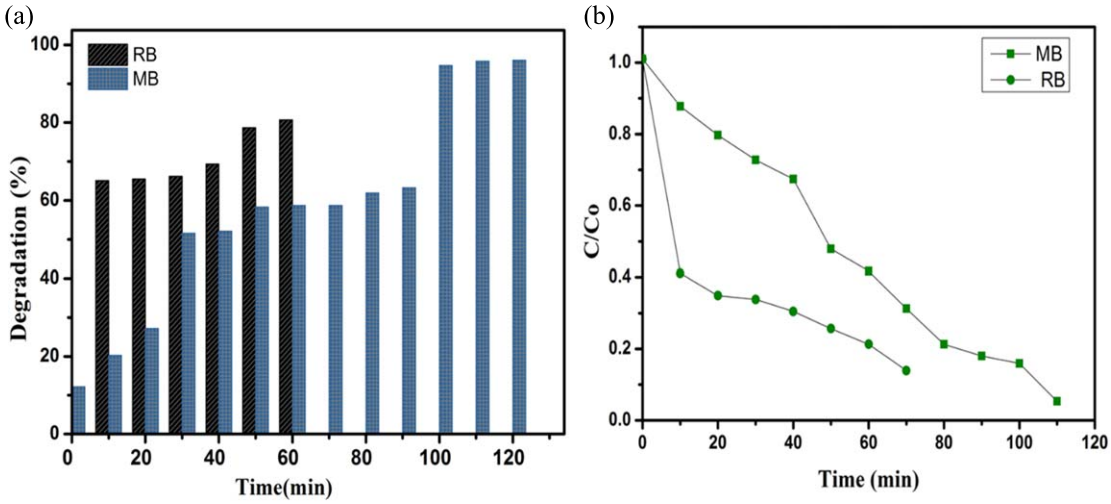

Figure 9. (a) The degradation efficiency for Methylene blue and RhodamineB. (b) Photocatalytic degradation of (MB) and (RB) under the irradiation of UV light over α-Mn_2O_3 nanorods.

figures 8(a), (b), respectively. Even after 30 min of irradiation time, the absorbance peak looked slightly changed, and there was no decolorization took place. However, the significant decrease in the absorbance spectrum and the effect of decolorization were observed in 30 min of irradiation when the α-Mn_2O_3 photocatalyst added with RB and MB.

Figure 9(a) shows the % of degradation of the MB and RB dye with different photocatalyst dosage. In order to compare the efficiency of photocatalyst, the % of degradation of MB at 120 min and RB at 70 min were estimated as 95% and 80%, respectively. The values were listed in table 1, which was compared with the earlier reports in table 2. Figure 9(b) shows the decreasing concentration of the MB and RB dye versus different illumination time intervals for the samples. It depicts that the good surface states and crystallinity of single-crystalline α-Mn_2O_3 nanorods improve the photocatalytic performance [27].

4.1. Decolorization of dye molecules mechanism

The schematic diagram in figure 10 represents the photocatalytic charge transfer taking place mechanism of α-Mn_2O_3 nanorods. Photocatalytic reaction was initiated by the photon incident on the photocatalyst, where the photoelectron excited from the valence band of a photocatalyst to the conduction band [39, 40]. The photoelectron excitation process leaves behind a hole in the valence band. The net result electron and hole pairs (e^-/h^+) generated as a photocatalyst equation (3).

Table 1. The optimized condition for the degradation of Methylene blue and Rhodamine blue using α- Mn_2O_3 nanorods and the degradation efficiency.

Parameters	Methylene blue	Rhodamine B	Degradation efficiency
Volume of the sample	100 ml	100 ml	
Initial concentration	2.5 mg	2.5 mg	
Weight of catalyst source	6.5 mg	4.5 mg	95% (MB)
Source	254 nm	254 nm	80% (RB)
Time taken for degradation	120 min	70 min	

Table 2. Comparison of α-Mn_2O_3 Nanorods by absorption with reported literature values.

Catalyst	Reaction time	Removal %	References
α- Mn_2O_3	120	90.2	[33]
CeO_2/V_2O_5	300	76.9	[34]
CeO_3/CuO	300	85.7	[35]
α- Bi_2O_3	360	30	[36]
NiO	300	70.2	[37]
Fe_2O_3/TiO_2	60	80	[38]
α- Mn_2O_3	240	71	[22]
α- Mn_2O_3	120	95	Present work
α- Mn_2O_3	70	80	Present work

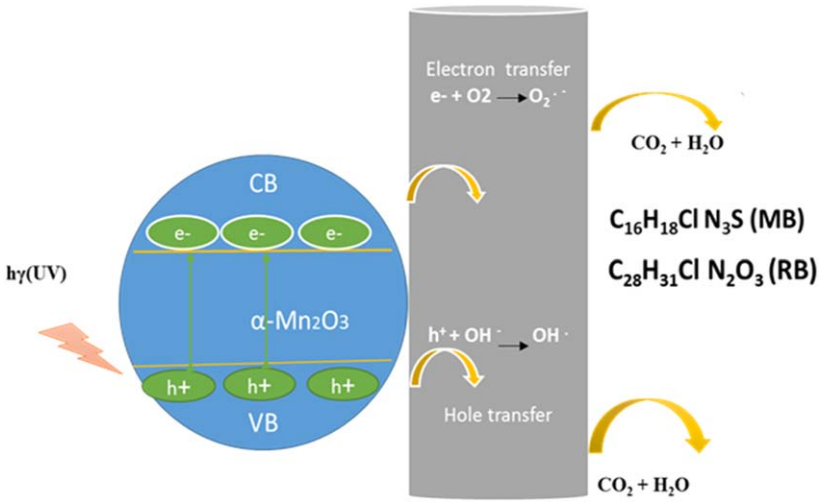

Figure 10. Photocatalytic dye degradation mechanism of α-Mn_2O_3.

$$Mn_2O_3 + h\nu(UV) \rightarrow Mn_2O_3 + h^+(VB) + e^-(CB) \quad (3)$$

While surface-bound water molecules react with the photogenerated hole (h^+_{VB}) to produce hydroxyl radicals. The hydroxyl radicals ($OH^·$) is a powerful oxidizing potential agent equation (5)

$$H_2O \rightarrow H^+ + OH^- \quad (4)$$

$$OH^- + h^+(VB) \rightarrow OH°(\text{Hydroxyl radicals}) \quad (5)$$

Electron in the conduction band is occupied by the oxygen in order to produce anionic superoxide radicals equation (6). This reduction and oxidation process is capable of degradation of the MB and RB under UV light [10, 41].

$$O_2 + e^-(CB) \rightarrow O_2^{\circ -} (\text{Anionic superoxide radicals}) \quad (6)$$

$$OH° + MB(\text{or})RB \rightarrow CO_{2\_} + H_2O \quad (7)$$

$$O_2^{\circ -} + RB(\text{or})MB \rightarrow CO_2 + H_2O \quad (8)$$

In the case of one- dimensional nanostructured α-Mn_2O_3 nanorods, the photogenerated electrons can traves along the length of the crystal as the space-charge region is well constructed in the longitudinal direction

[16]. The increase in the delocalization of electrons in α-Mn_2O_3 nanorods can lead to decrease in the probability of electron-hole pair recombination. This results in the existence of a large number of charge carriers on the active sites of α- Mn_2O_3 nanorod surface, which has better degradation efficiency as compared with spherical nanoparticles [17].

5. Conclusions

In summary, γ-MnOOH in the monoclinic phase has been synthesized by the hydrothermal method. A cubic bixbyite α-Mn_2O_3 nanorods were obtained by calcined γ-MnOOH at 600 °C for 4 h. XRD, SEM, TEM, and HRTEM showed the formation of cubic phase structure and well-defined large quality of rod-like morphology with a diameter of 318.4 nm length 8.15 μm, and growth mechanism of nanorods α-Mn_2O_3 was discussed. The decolorization of dye molecules performance for the methylene blue and rhodamine B dye solution under UV irradiation for 120 min and 70 min. The photocatalytic dye degradation efficiency was estimated as MB (95%), RB (80%). The results show that the degradation efficiency also depended on the photocatalyst dosage.

Acknowledgments

One of the authors CKS is thankful to VIT management for providing TRA ship and the corresponding author NKC is expressing his gratitude to VIT for granting seed money through RGEMS project.

ORCID iDs

Nirmala Grace Andrews https://orcid.org/0000-0002-2016-3013
Sudhagar Pitchaimuthu https://orcid.org/0000-0001-9098-8806
Krishna Chandar Nagamuthu Raja https://orcid.org/0000-0001-9759-5714

References

[1] Liu M, Wang Y, Cheng Z, Zhang M, Hu M and Li J 2014 Electrospun Mn_2O_3 nanowrinkles and Mn_3O_4 nanorods: morphology and catalytic application *Appl. Surf. Sci.* **313** 360–7
[2] Gupta V K, Ali I, Saleh T A, Nayak A and Agarwal S 2012 Chemical treatment technologies for waste-water recycling—an overview *RSC Adv.* **2** 6380–8
[3] Chong M N, Jin B, Chow C W K and Saint C 2010 Recent developments in photocatalytic water treatment technology: a review *Water Res.* **44** 2997–3027
[4] Zhao J, Nan J, Zhao Z and Li N 2017 Facile fabrication of novel Mn_2O_3 nanocubes with superior light-harvesting for ciprofloxacin degradation *Catal. Commun.* **102** 5–8
[5] Debabrata C and Shimanti D 2006 Visible light induced photocatalytic degradation of organic pollutants *J. Photochem. Photobiol.* **6** 186–205
[6] Gnanasekaran L, Hemamalini R, Saravanan R, Ravichandran K, Gracia F, Agarwal S and Gupta V K 2017 Synthesis and characterization of metal oxides (CeO_2, CuO, NiO, Mn_3O_4, SnO_2 and ZnO) nanoparticles as photo catalysts for degradation of textile dyes *J. Photochem. Photobiol. B Biol.* **173** 43–9
[7] Saravanan R, Karthikeyan N, Gupta V K, Thirumal E, Thangadurai P, Narayanan V and Stephen A 2013 ZnO/Ag nanocomposite: an efficient catalyst for degradation studies of textile effluents under visible light *Mater. Sci. Eng.* C **33** 2235–44
[8] Gui Z, Fan R and Chen X 2001 A simple direct preparation of nanocrystalline c -Mn_2O_3 at ambient temperature *Inorg. Chem. Commun.* **4** 294–6
[9] Salavati-niasari M, Mohandes F, Davar F and Saberyan K 2009 Fabrication of chain-like Mn_2O_3 nanostructures via thermal decomposition of manganese phthalate coordination polymers *Appl. Surf. Sci.* **256** 1476–80
[10] Gao Q and Liu Z 2017 FeWO4 nanorods with excellent UV–Visible light photocatalysis *Prog. Nat. Sci. Mater. Int.* **27** 556–556
[11] Deng J, He S, Xie S, Yang H, Liu Y, Guo G and Dai H 2015 Ultralow loading of silver nanoparticles on Mn_2O_3 nanowires derived with molten salts: a high-efficiency catalyst for the oxidative removal of toluene *Environ. Sci. Technol.* **49** 11089–95
[12] Cai Y, Liu S, Yin X, Hao Q, Zhang M and Wang T 2010 Facile preparation of porous one-dimensional Mn_2O_3 nanostructures and their application as anode materials for lithium-ion batteries *Phys. E Low-Dimensional Syst. Nanostructures* **43** 70–5
[13] Pérez-Garibay R, González-García A P, Fuentes-Aceituno J C, Rendón-Ángeles J C and Bello-Teodoro S 2016 Synthesis of Mn_2O_3 from manganese sulfated leaching solutions *Ind. Eng. Chem. Res.* **55** 9468–75
[14] Nassar M Y, Amin A S, Ahmed I S and Abdallah S 2016 Sphere-like Mn_2O_3 nanoparticles : facile hydrothermal synthesis and adsorption properties *J. Taiwan Inst. Chem. Eng.* **64** 79–88
[15] Byrappa K and Adschiri T 2007 Hydrothermal technology for nanotechnology *Prog. Cryst. Growth Charact. Mater.* **53** 117–66
[16] Zhang X, Qin J, Xue Y, Yu P, Zhang B, Wang L and Liu R 2014 Effect of aspect ratio and surface defects on the photocatalytic activity of ZnO nanorods *Sci. Rep.* **4** 4–11
[17] Upadhaya D and Dhar Purkayastha D 2020 Enhanced wettability and photocatalytic activity of seed layer assisted one dimensional ZnO nanorods synthesized by hydrothermal method *Ceram. Int.* **46** 1–9
[18] Chen Y, Zhang Y, Yao Q Z, Zhou G T, Fu S and Fan H 2007 Formation of α-Mn_2O_3 nanorods via a hydrothermal-assisted cleavage-decomposition mechanism *J. Solid State Chem.* **180** 1218–23
[19] Javed Q, Wang F P, Rafique M Y, Toufiq A M, Li Q S, Mahmood H and Khan W 2012 Diameter-controlled synthesis of α-Mn_2O_3 nanorods and nanowires with enhanced surface morphology and optical properties *Nanotechnology* **23** 415–603

[20] Gong P, Xie J, Fang D, He F, Li F and Qi K 2017 Study on the relationship between physicochemical properties and catalytic activity of Mn_2O_3 nanorods *Mater. Res. Express* **4** 115036
[21] Zhang Y, Chen J, Huang B and Li D 2011 Fabrication of Mn_2O_3 nanorods and their different paramagnetic properties *Adv. Mater. Res.* **233–235** 2252–7
[22] Gnanam S and Rajendran V 2013 Nanodumb-bells: structural, magnetic, optical and photocatalytic properties *J. Alloys Compd.* **550** 463–70
[23] Shao Y, Ren B, Jiang H, Zhou B, Lv L, Ren J, Dong L, Li J and Liu Z 2017 Dual-porosity Mn_2O_3 cubes for highly efficient dye adsorption *J. Hazard. Mater.* **333** 222–31
[24] Shen X, Ji Z, Miao H, Yang J and Chen K 2011 Hydrothermal synthesis of $MnCO_3$ nanorods and their thermal transformation into Mn_2O_3 and Mn_3O_4 nanorods with single crystalline structure *J. Alloys Compd.* **509** 5672–6
[25] Lin H B, Rong H B, Huang W Z, Liao Y H, Xing L D, Xu M Q, Li X P and Li W S 2014 Triple-shelled Mn_2O_3 hollow nanocubes: force-induced synthesis and excellent performance as the anode in lithium-ion batteries *J. Mater. Chem.* A **2** 14189–94
[26] Yuan Z Y, Ren T Z, Du G and Su B L 2004 A facile preparation of single-crystalline α-Mn_2O_3 nanorods by ammonia-hydrothermal treatment of MnO_2 *Chem. Phys. Lett.* **389** 83–6
[27] Deng B and Huang H Y 2014 Hydrothermal synthesis and characterisation of Mn_2O_3 nanowires *Adv. Mater. Res.* **1033–1034** 1040–3
[28] Murph S E H, Murphy C J, Leach A and Gall K 2015 A possible oriented attachment growth mechanism for silver nanowire formation *Cryst. Growth Des.* **15** 1968–74
[29] Krishna Chandar N and Jayavel R 2014 Structural, morphological and optical properties of solvothermally synthesized $Pr(OH)_3$ nanoparticles and calcined Pr_6O_{11} nanorods *Mater. Res. Bull.* **50** 417–20
[30] Chandar N K and Jayavel R 2012 Synthesis and photoluminescence properties of HMT passivated Dy_2O_3 nanoparticles *Phys. E Low-dimensional Syst. Nanostructures* **44** 1315–9
[31] Gnanam S and Rajendran V 2013 Facile hydrothermal synthesis of alpha manganese sesquioxide (α-Mn_2O_3) nanodumb-bells: structural, magnetic, optical and photocatalytic properties *J. Alloys Compd.* **550** 463–70
[32] Chandra S, Das P, Bag S, Bhar R and Pramanik P 2012 Mn_2O_3 decorated graphene nanosheet: an advanced material for the photocatalytic degradation of organic dyes *Mater.* **177** 855–61
[33] Cheng G, Yu L, Lin T, Yang R, Sun M, Lan B, Yang L and Deng F 2014 A facile one-pot hydrothermal synthesis of β-MnO_2 nanopincers and their catalytic degradation of methylene blue *J. Solid State Chem.* **217** 57–63
[34] Saravanan R, Joicy S, Gupta V K, Narayanan V and Stephen A 2013 Visible light induced degradation of methylene blue using CeO_2/V_2O_5 and CeO_2/CuO catalysts *Mater. Sci. Eng.* C **33** 4725–31
[35] Jalalah M, Faisal M, Bouzid H, Park J G, Al-Sayari S A and Ismail A A 2015 Comparative study on photocatalytic performances of crystalline α- and β-Bi_2O_3 nanoparticles under visible light *J. Ind. Eng. Chem.* **30** 183–9
[36] Ramesh M, Rao M P C, Anandan S and Nagaraja H 2018 Adsorption and photocatalytic properties of NiO nanoparticles synthesized via a thermal decomposition process *J. Mater. Res.* **33** 601–10
[37] Ahmed M A, El-Katori E E and Gharni Z H 2013 Photocatalytic degradation of methylene blue dye using Fe_2O_3/TiO_2 nanoparticles prepared by sol-gel method *J. Alloys Compd.* **553** 19–29
[38] Song L, Zhang S, Wu X and Wei Q 2012 A metal-free and graphitic carbon nitride sonocatalyst with high sonocatalytic activity for degradation methylene blue *Chem. Eng. J.* **184** 256–60
[39] Ajmal A, Majeed I, Malik R N, Idriss H and Nadeem M A 2014 Principles and mechanisms of photocatalytic dye degradation on TiO_2 based photocatalysts: a comparative overview *RSC Adv.* **4** 37003–26
[40] Pudukudy M and Yaakob Z 2016 Synthesis, characterization, and photocatalytic performance of mesoporous α-Mn_2O_3 microspheres prepared via a precipitation route *J. Nanoparticles* **2016** 1–7
[41] Cao J, Mao Q and Qian Y 2012 Synthesis of Mn_2O_3 homogeneous core/hollow-shell structures with excellent adsorption performance *J. Solid State Chem.* **191** 10–4